Science Bulletin 69 (2024) 1020–1026

Contents lists available at ScienceDirect

Science Bulletin

journal homepage: www.elsevier.com/locate/scib

Article

The arrival time and energy of FRBs traverse the time-energy bivariate space like a Brownian motion

Yong-Kun Zhang [a,b,c], Di Li [a,b,c,d,e,*], Yi Feng [d], Pei Wang [a,b,f], Chen-Hui Niu [g], Shi Dai [h], Ju-Mei Yao [i,j,k], Chao-Wei Tsai [a,b,c,f]

[a] National Astronomical Observatories, Chinese Academy of Sciences, Beijing 100101, China
[b] Key Laboratory of Radio Astronomy and Technolgoy, Chinese Academy of Sciences, Beijing 100101, China
[c] University of Chinese Academy of Sciences, Beijing 100049, China
[d] Research Center for Astronomical Computing, Zhejiang Laboratory, Hangzhou 311100, China
[e] New Cornerstone Science Laboratory, Shenzhen 518054, China
[f] Institute for Frontiers in Astronomy and Astrophysics, Beijing Normal University, Beijing 102206, China
[g] Institute of Astrophysics, Central China Normal University, Wuhan 430079, China
[h] School of Science, Western Sydney University, Penrith NSW 2751, Australia
[i] Xinjiang Astronomical Observatory, Chinese Academy of Sciences, Urumqi 830011, China
[j] Key Laboratory of Radio Astronomy, Chinese Academy of Sciences, Urumqi 830011, China
[k] Xinjiang Key Laboratory of Radio Astrophysics, Urumqi 830011, China

ARTICLE INFO

Article history:
Received 24 April 2023
Received in revised form 22 November 2023
Accepted 2 February 2024
Available online 9 February 2024

Keywords:
Fast radio burst
Earthquake
Stochastic
Chaos

ABSTRACT

The origin of fast radio bursts (FRBs), the brightest cosmic explosion in radio bands, remains unknown. We introduce here a novel method for a comprehensive analysis of active FRBs' behaviors in the time-energy domain. Using "Pincus Index" and "Maximum Lyapunov Exponent", we were able to quantify the randomness and chaoticity, respectively, of the bursting events and put FRBs in the context of common transient physical phenomena, such as pulsar, earthquakes, and solar flares. In the bivariate time-energy domain, repeated FRB bursts' behaviors deviate significantly (more random, less chaotic) from pulsars, earthquakes, and solar flares. The waiting times between FRB bursts and the corresponding energy changes exhibit no correlation and remain unpredictable, suggesting that the emission of FRBs does not exhibit the time and energy clustering observed in seismic events. The pronounced stochasticity may arise from a singular source with high entropy or the combination of diverse emission mechanisms/sites. Consequently, our methodology serves as a pragmatic tool for illustrating the congruities and distinctions among diverse physical processes.

1. Introduction

Fast radio bursts (FRBs) are intense pulses of radio emission that last just a few milliseconds. First discovered in 2007 [1], FRBs have since been observed by a variety of radio telescopes around the world. Despite their ubiquity, however, the origin of these mysterious signals remains unknown. FRBs have a wealth of observational parameters carrying information about the sources and the propagation paths, including arrival time, energy, duration, bandwidth, polarization, dispersion, scintillation, scattering, etc. Recent studies on the polarization of FRBs suggest that FRBs are located in complex magnetized environments [2–5]. These studies demonstrate information about the propagation paths of FRBs. Time and energy are two observational parameters directly related to the radiation nature of FRBs. The observation of FRB 20121102A with the Five-hundred-meter Aperture Spherical radio Telescope (FAST) for the first time revealed a bimodal distribution of FRB energy, suggesting that there may be different radiation mechanisms for FRBs [6,7].

The study of time and energy sequences of repeating FRB bursts enables a deeper understanding of the origin of FRBs, which is difficult to achieve with non-repeating bursts because their only burst is just a point in time-energy phase space. Here, we use two active repeating FRBs as our analysis objects, which are the only two FRBs known to have associated compact persistent radio sources (PRSs) [8–10], namely FRB 20121102A and FRB 20190520B. Both have gone through highly active episodes over a substantial dynamic range of time scales (milliseconds to

* Corresponding author.
E-mail address: dili@nao.cas.cn (D. Li).

https://doi.org/10.1016/j.scib.2024.02.010

months), as detected by FAST [6,10]. Due to the high sensitivity and high cadence coverage of FAST's observations of these two FRBs, we can obtain more complete event series than other telescopes. We report here a first systematic examination of the FRB behaviors in the time-energy bivariate domain.

2. Data

FRB 20121102A was the first FRB found to be repeating and to be precisely localized [8,11,12]. In one extremely active epoch, FAST detected 1652 pulses from FRB 20121102A between August 29 and October 29, 2019 [6]. Since then, we have been carrying out regular monitoring of FRB 20121102A once every one or two months. On August 17 and 23, 2020, FAST caught another 12 bursts. Since then, no more burst has been detected. FRB 20190520B is the first repeating FRB discovered by FAST during the Commensal Radio Astronomy FAST Survey (CRAFTS) [13], which has been accurately located with a PRS [10]. Since its discovery on May 20th, 2019, more than 200 pulses have been detected by FAST and Parkes [5]. Fig. 1 shows the observation coverage and the detected bursts of FRB 20121102A and FRB 20190520B.

3. Time domain analysis and results

We employed the Lomb-Scargle Periodogram (LSP) [14,15] to search for periods of FRB 20121102A and FRB 20190520B, yet no statistically significant period signals were identified within the range of 1 ms to 1000 s. To quantify the significance (signal-to-noise ratio, S/N) of signals at different periods, we compared the power differences between randomly generated time series and the time series of FRB bursts in the LSP. For FRB 20121102A, we generated a time series with the same number as the FRB bursts between the time of the first and last burst's arrival time, drawn from a uniform distribution. Subsequently, we applied the LSP to this randomly generated sequence. We repeated this process 100 times, resulting in a distribution of periodogram powers for random signals at different periods. We conducted the same procedure for FRB 20190520B. Within the range of 1 ms to 1000 s, no significant periodic signals for both FRBs surpassed 5σ of the distribution of periodogram powers from the random time series (Fig. 2). Thus we have significantly constrained the possibility of periodic signal existence. Several effects, including variable emission altitudes/sites, may complicate the inference of a magnetar's spin period from the arrival times of FRB bursts [16]. An alternative interpretation could be that the period of the magnetar powering FRB is much longer than that of Galactic magnetars, so there is no short-timescale periodicity in the FRB data [17]. Regardless of the specific cause, the absence of a detected periodic signal still highlights the inherent randomness in the emission of FRBs.

We now look into the more fundamental aspects of FRBs' time-domain behaviors through analysis of waiting times. The waiting time between two events is $\delta = t_{i+1} - t_i$, where t_{i+1} and t_i are the arrival times for the $(i+1)_{\rm th}$ and $i_{\rm th}$ events, respectively.

Since the discovery of FRB 20200428, the origin of FRBs being from magnetars has gradually gained popularity [18,19]. As a possible source model for FRBs, the production of FRBs by magnetars relies on some trigger mechanisms [20], including crust cracking at the neutron star surface [7,21,22], sudden magnetic reconnection events in the magnetosphere [23], or triggers from external events [24,25]. Motivated by this, we compared FRBs with earthquake and solar flare with similar but not identical mechanisms.

The seismic data are from the Southern California Earthquake Data Center [26], which contains information such as the occurrence time, latitude, longitude, and magnitude of the earthquake since 1932. For earthquake, we selected events within a region of $2^\circ \times 2^\circ$ as a continuous seismic sequence. The magnitudes of all earthquakes are converted into energy (erg) through an empirical relation [27]. Solar flare data are from the Hinode Flare Catalogue [28]. We simulated a 100-step Brownian motion. In mathematics, Brownian motion is described by the Wiener process, a stochastic process $W(t)$ concerning time t. According to the definition of Brownian motion, for time t and s, the increments of Brownian motion $W(t) - W(s)$ follow a normal distribution $\mathcal{N}(0, t-s)$. Therefore, our simulation proceeded as follows: Firstly, we sampled the waiting time δt for each step of the Brownian motion from the exponential distribution $P(t) = \lambda e^{-\lambda t}$, where $\lambda = 1$, corresponding to a Poisson process with an event rate of 1. Subsequently, based on each step's waiting time, we sampled the step size from the normal distribution $\mathcal{N}(0, {\rm d}t)$.

The waiting time distributions of these phenomena are presented in Fig. 3a–e. We defined an average time as $\bar{T} = \sum T_i / \sum N_i$, where T_i and N_i are the length and event count of the observation session. All waiting times are normalized by corresponding $\bar{T}$. For fitting the waiting time distribution, we employed the EMCEE package to perform maximum likelihood estimation on the fitting parameters. We define the likelihood function as

$$L(\theta|t) = \sum_i \log f(t,\theta), \tag{1}$$

where t is the waiting times, $f(t,\theta)$ is the model for waiting time distribution, and θ is the free parameter(s) for the model. $f(t,\theta)$ could be

- Weibull distribution
  $f(t,\theta) = f(t,k,\lambda) = \frac{k}{\lambda}\left(\frac{t}{\lambda}\right)^{k-1} e^{-(t/\lambda)^k}$, where θ represents the shape parameter k and the scale parameter λ.
- Log-normal distribution
  $f(t,\theta) = f(t,\mu,\sigma) = \frac{1}{x\sigma\sqrt{2\pi}} \exp\left[-\frac{(\ln x-\mu)^2}{2\sigma^2}\right]$, where θ represents the expected value μ and standard deviation σ of the variable's natural logarithm.
- Exponential distribution
  $f(t,\theta) = f(t,\lambda) = \lambda e^{-\lambda t}$, where θ represents the event rate λ.
- Mixture of two exponential distributions
  $f(t,\theta) = f(t,\lambda_1,\lambda_2,p) = p e^{-\lambda_1 t} + (1-p/\lambda_1)\lambda_2 e^{-\lambda_2 t}$, where θ representing two event rates $\lambda_{1,2}$ and a proportionality factor p.

The waiting time distribution for a Poisson process follows an exponential distribution. The waiting time distribution of the earthquake deviates from the exponential distribution and can be better described by a Weibull distribution. This means that earthquake events with shorter waiting times occur more frequently than expected from a simple Poisson process, i.e., clustering in time. The waiting time distribution of solar flare can be fitted by a log-normal function, which means the event rate of solar flare changes randomly.

Regarding the waiting time of FRBs, the earlier assumption was a non-stationary Poisson process or a Weibull distribution [29,30], albeit influenced by the sparse sampling of early burst events. As depicted in Fig. 3, the bimodal waiting time distribution of FRBs evidently differs from a single Weibull distribution, which can be well applied to earthquake events. There are also diverse models used to describe the distribution of waiting times for FRBs, including LogNormal distribution [31], Weibull [32], time-dependent Poisson processes [33,34].

For comparative analysis, using FRB 20121102A as an example, we selected waiting times exceeding 1 s. Fitting was undertaken with exponential (corresponding to a Poisson process), Weibull, and lognormal functions. The goodness of fit was assessed using

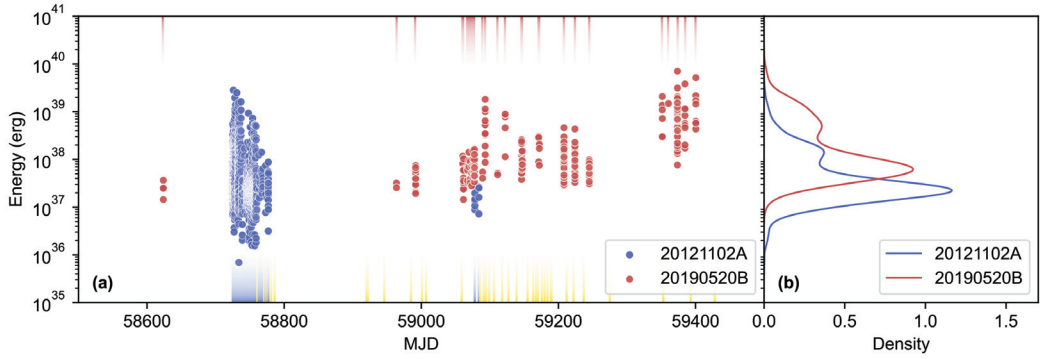

Fig. 1. The detected bursts with energy from FRB 20121102A and FRB 20190520B. (a) The blue dots and red dots show the energy and arrival time of bursts from the two FRBs. The blue and red bars are the observation session of the two FRBs with detection, and the yellow bars are the observation session without detection. (b) The kernel density estimate (KDE) energy distribution of the two FRBs.

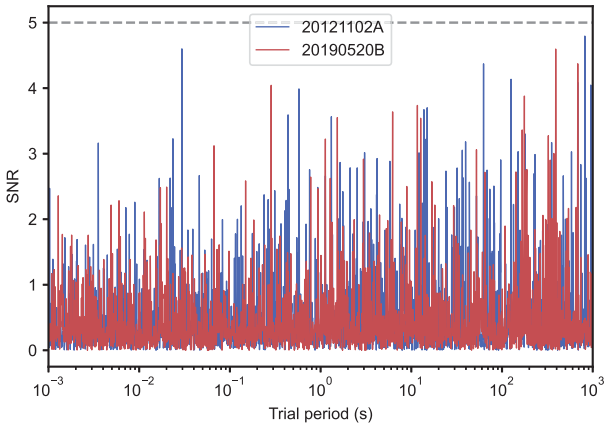

Fig. 2. The periodogram of FRB 20121102A and FRB 20190520B.

adjusted R-squared, which provides a refined assessment of the model's fitting effectiveness by accounting for the number of independent variables utilized. The parameter counts for exponential, Weibull, and lognormal are 1, 2, and 2, respectively. The calculated adjusted R-squared values were 0.920, 0.917, and 0.906 for these three functions. While all three functions appear adept at modeling FRB waiting times, we lean toward the simplest model, the exponential (Poisson process) function, for describing the distribution of FRB waiting times. The time-dependent Poisson process, which is the sum of multiple Poisson processes, entails a greater number of parameters and evidently excels in fitting residuals compared with models with fewer parameters. Nevertheless, under the simplest conditions, our results indicate the effectiveness of a single Poisson process. Consequently, in this context, we opt for employing two Poisson processes to fit the entire distribution of FRB waiting times.

We also explored the distribution of waiting times under different energy thresholds. Taking FRB 20121102A as an example, we set a series of energy thresholds, calculated the waiting time distribution for each, and employed an exponential function to fit the two peaks of waiting times. For exponential distributed waiting times, $P(t) = \lambda e^{-\lambda t}\,dt = \lambda e^{-\lambda t} t\,d\log t$, the peak corresponds to the position where the derivative is zero $P'(t) = 0 \Rightarrow t = 1/\lambda$. Thus, the exponential distribution provides the typical waiting time corresponding to the peak. In Fig. 3g, h, we present the characteristic times corresponding to the two peaks of waiting time under different energy thresholds. The left peak (short timescale waiting times) is insensitive to the choice of energy threshold, implying an intrinsic correlation with the radiation mechanism. The right peak (long timescale waiting times) strongly depends on the energy threshold or the detected event number. As the energy threshold increases, it leads to a decrease in the detected bursts, resulting in longer waiting times. In panel H, two inflection points correspond to the two peaks in the energy distribution. After normalizing the right peak's waiting time using the detected number of bursts under different energy thresholds and observation duration, we can see that all the normalized right peaks hover around 1, indicating that the right peak is a stochastic process relying on sampling (event rate). When the waiting time of FRBs can be described by stochastic processes, it further disfavors the prospect of (quasi)-periodicity in FRBs.

The distinct characteristics of the waiting time distribution underscore that the emission of FRBs is not like seismic events. A recent study has proposed a semblance of aftershock characteristics between FRBs and earthquakes through a custom correlation function [35]. However, the similarity in the "correlation function" between earthquakes and FRBs arises from the bias of waiting time distributions from one Poisson process. Here, we show that despite both earthquakes and FRBs deviating from a Poisson process in terms of waiting times, the manner of deviation differs. Therefore, it is hard to conclude that FRBs exhibit seismic aftershock characteristics. This assertion is further substantiated in our subsequent analysis of energy distribution.

4. Energy domain analysis and results

Despite the common perception of randomly occurring earthquakes, seismic events cluster in time and magnitude [36–38]. The deviation of earthquakes from randomness origins from its nonlinear dynamical systems [36,39]. Assuming in an event series, the subsequent event often possesses lower energy than its predecessor. After shuffling, the probability of subsequent energy being lower than the predecessor will decrease. Based on this fact, we adopted the analysis method used in ref. [38] for earthquakes.

Consider conditional probability

$$P(\Delta m_i < m_0 | \Delta t_i < t_0) = \frac{N(\Delta m_i < m_0, \Delta t_i < t_0)}{N(\Delta t_i < t_0)}\,, \tag{2}$$

where $\Delta t_i = t_{i+1} - t_i$ and $\Delta m_i = m_{i+1} - m_i$ are the temporal and magnitude difference between subsequent events, $N(\cdots)$ is the number of pairs of subsequent events satisfying the conditions specified in parentheses.

With fixed m_0 and t_0, the quantity $P(\Delta m_i^* < m_0 | \Delta t_i < t_0)$ for independent reshuffled series are calculated, where $\Delta m_i^* = m_{i+1}^* - m_i^*$ is the magnitude difference between subsequent events of reshuffled series. We employed NUMPY.RANDOM.SHUFFLE to

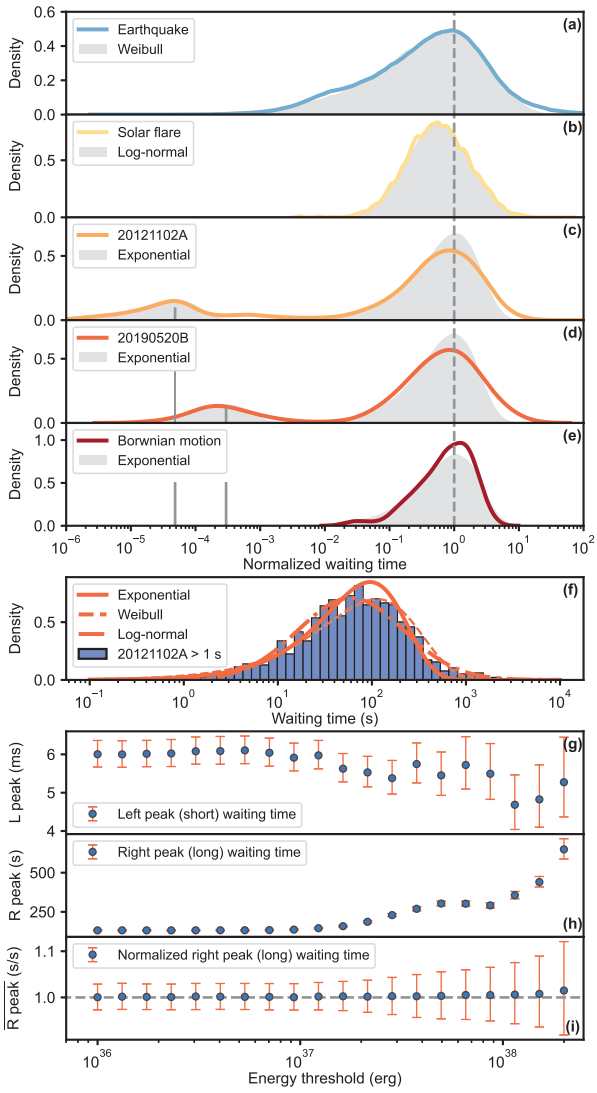

Fig. 3. The normalized waiting time distribution of earthquake, solar flare, two FRBs, and Brownian motion. Colored lines in (a–e) are the KDEs of waiting times for these phenomena, which are normalized by $\bar{T}$ of 3435.1, 25810.4, 88.4, 123.3, and 190.4 s, respectively. Gray regions in (a–e) indicate the fitting of waiting times with Weibull function, LogNormal function, and Exponential function (Poisson process). The gray solid lines denote the short characteristic waiting time of the two FRBs, which are ∼4 ms for FRB 20121102A and ∼36 ms for FRB 20190520B. (f) The distribution of waiting times longer than 1 s for FRB 20121102A. The solid line, dashed line, and dash-dot line denote the fitting results of the exponential function, Weibull function, and lognormal function, respectively. (g–i) The left peak, right peak, and normalized right peak of waiting time under different energy thresholds.

rearrange our event series, which is based on the Fisher-Yates shuffle algorithm to produce an unbiased permutation. The central limit theorem makes the quantity $P(\Delta m_i^* < m_0|\Delta t_i < t_0)$ a Gaussian distribution with mean value $\mu(m_0,t_0)$ and standard deviation $\sigma(m_0,t_0)$. The biases between $\mu(m_0,t_0)$ and $P(\Delta m_i < m_0|\Delta t_i < t_0)$ for earthquake, FRB 20121102A and FRB 20190520B are $5.65\sigma, 0.79\sigma$ and 0.40σ (Fig. 4a–c), respectively. Generally, the detection of earthquakes is more complete than that of FRBs. Here, we conducted a test related to earthquake magnitude thresholds. For FRB 20121102A, the burst with the highest energy differs by a factor of 4000 from the one with the lowest energy, and for FRB 20190520B, the factor is 500. In the earthquake data, the highest magnitude is 7.5. By progressively increasing the energy threshold, we made the lowest-energy earthquake event reach 1/500 of the highest-energy event. Throughout this process, we calculated the S/N of the hypothesis "the energy of the subsequent event is lower than that of the preceding event" for different thresholds. In Fig. 4d, we can see that even when compressing the dynamic range of earthquake energies to 1/500, the S/N still exceeds 2, far surpassing the two FRBs. This indicates that no clustering in the energy of FRB bursts. Simply put, there is no excess number of bursts following a bright one, while there are more after-quakes following a major event than pre-quakes.

5. Stochasticity and chaos

In dynamical studies, chaos and stochasticity are two distinct concepts. Chaos is characterized by unpredictability that increases with time, whereas stochasticity's unpredictability remains stable over time. We use "Pincus Index" ($\mathcal{PI}$) and "Maximum Lyapunov exponent" ($\mathcal{MLE}$), respectively, to quantify the stochasticity and chaos of event sequences.

The $\mathcal{PI}$ is used to describe the degree of stochasticity based on the Max Approximate Entropy ($\mathcal{MAE}$) [40,41], by measuring the change in information entropy before and after shuffling a sequence. $\mathcal{PI}$ is zero for completely ordered systems and one for totally random systems. For an event series $\{e_i\}_{i=1,\cdots,N}$, the $\mathcal{MAE}$ [40,41] can be defined as

$$\mathcal{MAE} = \max_r \left(-\frac{1}{N-m}\sum_{i=1}^{N-m} \log \frac{\sum_{j=1}^{N-m} \mathrm{dist}(x_j,x_i) < r}{N-m} \Bigg|_m^{m+1} \right), \tag{3}$$

where $X = \{x_i\}_{i=1,\cdots,N-m} = \{\{e_1,\cdots,e_{1+m}\},\cdots,\{e_{N-m},\cdots,e_N\}\}$ is the reorganized sequence of the initial event series, N is the length of the initial event series, $\mathrm{dist}(x_j,x_i)$ is the distance between each pair of the reorganized sequence X, and r is the distance threshold. $\mathcal{MAE}$ quantifies the greatest difference in information between the segments of length m and $m+1$, which needs to obtain a max entropy of the recombination sequence by changing different thresholds r. For making the $\mathcal{MAE}$ comparable between series, the $\mathcal{PI}$ was defined as

$$\mathcal{PI} = \frac{\mathcal{MAE}_{\mathrm{initial}}}{\mathcal{MAE}_{\mathrm{shuffled}}}. \tag{4}$$

After calculating the $\mathcal{MAE}$ or called $\mathcal{MAE}_{\mathrm{initial}}$ for initial event series, we randomly reshuffled the series and calculated $\mathcal{MAE}$ for 100 times. The median value is $\mathcal{MAE}_{\mathrm{shuffled}}$, the standard deviation value is used to define the error of $\mathcal{PI}$. In the calculation of the $\mathcal{PI}$, the distance metric used is the Euclidean distance. To preserve the original sequence information as much as possible and minimize the introduction of artificial bias, we linearly mapped both the time and energy sequences to the range of 0 to 1 simply.

The $\mathcal{MLE}$ represents the degree of dispersion of trajectories in phase space and is a numerical characteristic used to identify chaotic behavior in a nonlinear system [42]. $\mathcal{MLE}$ less than 0 corresponds to a periodic motion or a stable system that is static in time-energy space. $\mathcal{MLE}$ greater than 0 indicates the existence of chaos. We use NOLDS [43] method for $\mathcal{MLE}$ calculation. As the $\mathcal{MLE}$ is the maximum value of the whole spectrum of Lyapunov exponents, it is difficult to define an error.

The $\mathcal{PI}$ and $\mathcal{MLE}$ values are shown in Fig. 5a. The pulsar data used here were a pulsar named J1840 + 2843 discovered within the CRAFTS project [1]. As expected, the most regular motion is a sine-wave, with small values in both, followed by pulsar with representative $\mathcal{PI}\sim$0.4 and $\mathcal{MLE}\sim$0.08. Earthquakes are most chaotic

[1] http://groups.bao.ac.cn/ism/CRAFTS/202203/t20220310_683697.html.

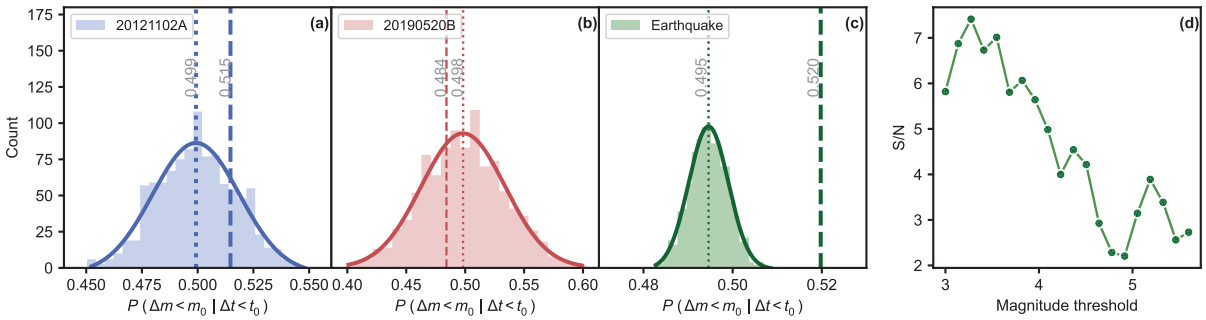

Fig. 4. The probability (P) of the hypothesis "the energy of the subsequent event is lower than that of the preceding event". (a–c) The probability (P) of the original event sequences (dashed lines) for FRB 20121102A (blue), FRB 20190520B (red), and earthquakes (green). The histogram and the dotted lines show the distribution and median of this probability (P) of randomly shuffled event sequences. (d) The variation in the S/N of the probability (P) under different earthquake magnitude thresholds.

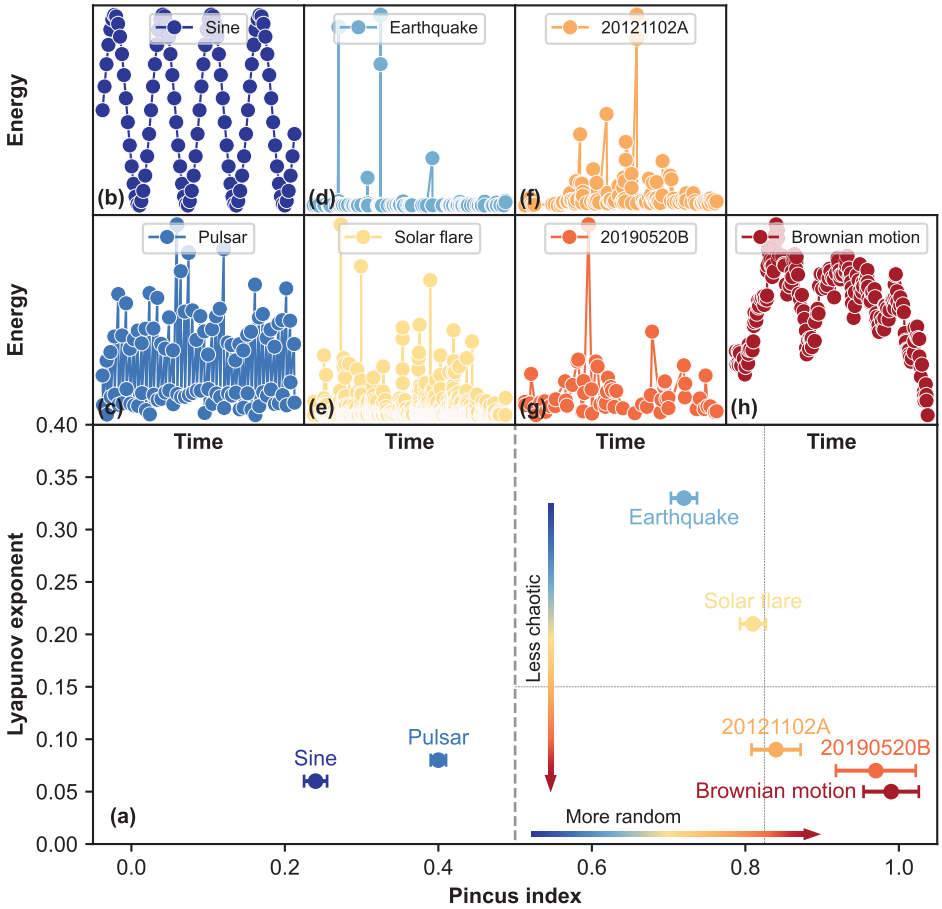

Fig. 5. The Pincus index vs. Lyapunov exponent of sine function, pulsar, earthquake, solar flare, FRB 20121102A, FRB 20190520B and Brownian motion. The top and middle panels present event series in time-energy space of these sources. The color changes from blue to red, implying increased stochasticity. ($\mathcal{PI}, \mathcal{MLE}$) value is (0.24, 0.06) for sine-wave, (0.40, 0.08) for pulsar, (0.72, 0.33) for Earthquake, (0.81, 0.21) for solar flare, (0.84, 0.09) for FRB 20121102A, (0.97, 0.07) for FRB 20190520B, and (0.99, 0.05) for Brownian motion. See the video file in Supplementary materials.

with $\mathcal{MLE}$~0.33. Solar flares are less chaotic, but more random than earthquakes. FRBs are even more random ($\mathcal{PI}$~0.84–0.97) and less chaotic ($\mathcal{MLE}$~0.07–0.09) than solar flares, mimicking Brownian motion ($\mathcal{PI}$~0.99) that is the most random in the bivariate time-energy space, among the systems considered here.

To ascertain the robustness of our calculations, we considered two types of tests. In the calculation of the $\mathcal{PI}$, only the parameter m remains as a free variable. We conducted tests by adopting $m \in \{2, 3, 4, 5\}$. As depicted in Fig. 6a, the deviation of the $\mathcal{PI}$ did not exceed 0.1 for different values of m. Even with slight variations in the $\mathcal{PI}$, the relative relationships among different physical phenomena remained unchanged when the same m was selected. Additionally, given that the detection of these physical phenomena cannot be exhaustive, we further examined the impact of sequence completeness on the results of the $\mathcal{PI}$ and $\mathcal{MLE}$ calculations. By adjusting the energy threshold, we retained different proportions of events (ranging from 100% down to 50%) and subsequently computed the $\mathcal{PI}$ and $\mathcal{MLE}$ for each case. From retaining 100% of the events to selecting only those with the top 50% energy levels, the $\mathcal{PI}$ and $\mathcal{MLE}$ exhibited remarkable stability (Fig. 6b, c), confirming the robustness of our calculations.

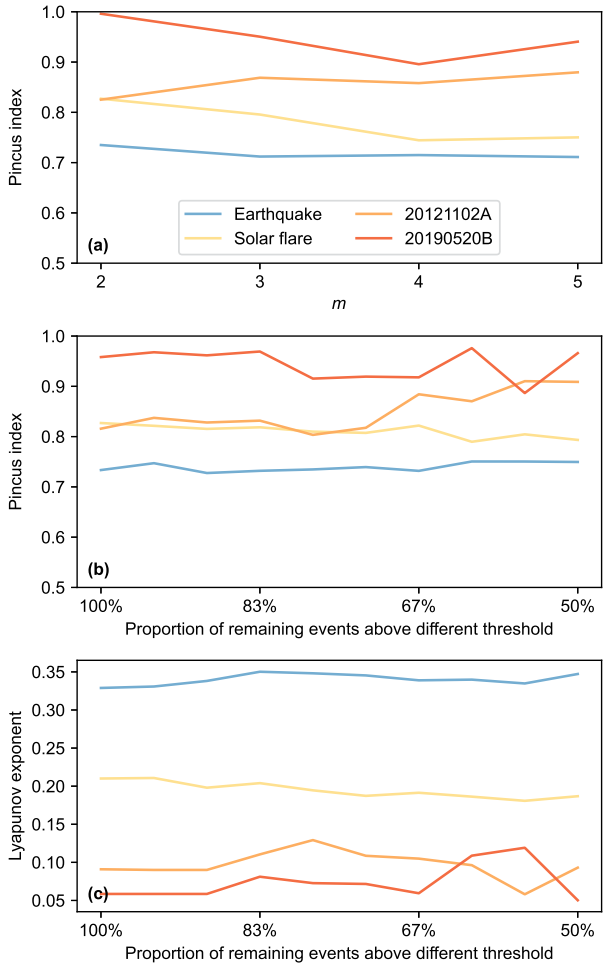

Fig. 6. The robustness test of $\mathcal{PI}$ and $\mathcal{MLE}$. (a) The $\mathcal{PI}$ values using different segments of length m. (b, c) The $\mathcal{PI}$ and $\mathcal{MLE}$ under different energy thresholds.

Our analysis reveals that active repeaters congregate with Brownian motion toward highly random, yet less chaotic regions in the stochasticity-chaos phase space (Fig. 5a). This is distinct from earthquakes and solar flares, both of which are more chaotic but less random than FRBs. Additionally, as previously analyzed, earthquakes exhibit time and energy clustering behavior (Figs. 3, 4). FRBs, however, do not show clustering in neither time nor energy. The random paths of FRB events in time-energy space favor origin models based on complex processes, such as in a thermodynamic system, the movement or diffusion of molecules is akin to the phenomenon of interest.

6. Conclusion

In summary, using $\mathcal{PI}$ and $\mathcal{MLE}$ to quantify the stochasticity and chaos of event sequences may be an effective method for intuitively demonstrating the similarities and differences between various physical processes. Specifically, here we compare FRBs, pulsar, solar flares, earthquakes, and Brownian motion in the stochasticity-chaos phase space. The strong stochasticity, akin to Brownian motions, of active repeaters with PRS counterparts, along with the growing evidence of their multi-variate behaviors, such as their bimodal energy distribution [6,7,44,45], could be generated by a single source with high information entropy or the combination of multiple radiation mechanisms or emission sites. Either way, it is unlikely that active repeating FRBs originate from a stably spin compact objects within a clean environment.

Conflict of interest

The authors declare that they have no conflict of interest.

Acknowledgments

This work made use of the data from FAST (Five-hundred-meter Aperture Spherical radio Telescope). FAST is a Chinese national mega-science facility, operated by National Astronomical Observatories, Chinese Academy of Sciences. This work was supported by the Open Project Program of the Key Laboratory of FAST, Chinese Academy of Sciences. The Parkes radio telescope (Murriyang) is part of the Australia Telescope National Facility, which is funded by the Commonwealth of Australia for operation as a National Facility managed by CSIRO. This work was partly carried out by using Hinode Flare Catalogue (https://hinode.isee.nagoya-u.ac.jp/flare_catalogue/), which is maintained by ISAS/JAXA and Institute for Space-Earth Environmental Research (ISEE), Nagoya University. Yong-Kun Zhang thanks Wei-Yang Wang for the comments about the star-quake model.

Di Li and Yi Feng are supported by the National Natural Science Foundation of China (NSFC) (11988101, 11725313, 11690024, and 12203045), and the Key Research Project of Zhejiang Lab (2021PE0AC03). Di Li is a New Cornerstone Investigator. Pei Wang is supported by NSFC (fU2031117), the Youth Innovation Promotion Association CAS (ID. 2021055) and the Cultivation Project for FAST Scientific Payoff and Research Achievement of CAMS-CAS. Chen–Hui Niu is supported by NSFC (12203069), the National SKA Program of China (2022SKA0130100), and the Office Leading Group for Cyberspace Affairs, CAS (CAS-WX2023PY-0102). Shi Dai is the recipient of an Australian Research Council Discovery Early Career Award (DE210101738) funded by the Australian Government. Ju-Mei Yao was supported by the National Science Foundation of Xinjiang Uygur Autonomous Region (2022D01D85), the Major Science and Technology Program of Xinjiang Uygur Autonomous Region (2022A03013-2), the Tianchi Talent project, and the CAS Project for Young Scientists in Basic Research (YSBR-063).

Author contributions

Yong-Kun Zhang and Di Li developed the concept of the manuscript. Yong-Kun Zhang conducted the data analysis and visualization. Pei Wang, Chen–Hui Niu, Shi Dai, and Yong-Kun Zhang searched the new bursts and analysed the burst properties. Yong-Kun Zhang, Di Li, Chao-Wei Tsai, Ju-Mei Yao, and Yi Feng led the discussion on the interpretation of the results and writing of the manuscript. All authors contributed to the analysis or interpretation of the data and the final version of the manuscript.

Appendix A. Supplementary materials

Supplementary materials to this article can be found online at https://doi.org/10.1016/j.scib.2024.02.010.

Data availability

Earthquake data from the Southern California Earthquake Data Center are used in this paper. The full dataset and documentation can be downloaded from https://dx.doi.org/10.7909/C3WD3xH1. Solar flare data from Hinode Flare Catalogue are used in this paper. The full dataset and documentation can be downloaded from

https://doi.org/10.34515/CATALOG.HINODE-00000. Other data and a visualization of the movement of FRB and earthquake in time-energy space can be accessed in ScienceDB https://doi.org/10.57760/sciencedb.09716.

References

[1] Lorimer DR, Bailes M, McLaughlin MA, et al. A bright millisecond radio burst of extragalactic origin. Science 2007;318:777.
[2] Beniamini P, Kumar P, Narayan R. Faraday depolarization and induced circular polarization by multipath propagation with application to FRBs. Mon Not R Astron Soc 2022;510:4654–68.
[3] Feng Y, Li D, Yang YP, et al. Frequency-dependent polarization of repeating fast radio bursts—implications for their origin. Science 2022;375:1266–70.
[4] Xu H, Niu JR, Chen P, et al. A fast radio burst source at a complex magnetized site in a barred galaxy. Nature 2022;609:685–8.
[5] Anna-Thomas R, Connor L, Dai S, et al. Magnetic field reversal in the turbulent environment around a repeating fast radio burst. Science 2023;380:599–603.
[6] Li D, Wang P, Zhu WW, et al. A bimodal burst energy distribution of a repeating fast radio burst source. Nature 2021;598:267–71.
[7] Yang YP, Zhang B. Fast radio bursts and their high-energy counterparts from magnetar magnetospheres. Astrophys J 2021;919:89.
[8] Chatterjee S, Law CJ, Wharton RS, et al. A direct localization of a fast radio burst and its host. Nature 2017;541:58–61.
[9] Marcote B, Paragi Z, Hessels JWT, et al. The repeating fast radio burst FRB 121102 as seen on milliarcsecond angular scales. Astrophys J Lett 2017;834:L8.
[10] Niu CH, Aggarwal K, Li D, et al. A repeating fast radio burst associated with a persistent radio source. Nature 2022;606:873–7.
[11] Spitler LG, Scholz P, Hessels JWT, et al. A repeating fast radio burst. Nature 2016;531:202–5.
[12] Tendulkar SP, Bassa CG, Cordes JM, et al. The host galaxy and redshift of the repeating fast radio burst FRB 121102. Astrophys J Lett 2017;834:L7.
[13] Li D, Dickey JM, Liu S. Preface: Planning the scientific applications of the five-hundred-meter aperture spherical radio telescope. Res Astron Astrophys 2019;19:016.
[14] Lomb NR. Least-squares frequency analysis of unequally spaced data. Astrophys Space Sci 1976;39:447–62.
[15] Scargle JD. Studies in astronomical time series analysis. II. Statistical aspects of spectral analysis of unevenly spaced data. Astrophys J 1982;263:835–53.
[16] Cordes JM, Wasserman I, Chatterjee S, et al. Empirical assessment of aperiodic and periodic radio bursts from young precessing magnetars. Astrophys J 2022;929:97.
[17] Beniamini P, Wadiasingh Z, Metzger BD. Periodicity in recurrent fast radio bursts and the origin of ultralong period magnetars. Mon Not R Astron Soc 2020;496:3390–401.
[18] Collaboration CHIME/FRB, Andersen B C, et al. A bright millisecond-duration radio burst from a Galactic magnetar. Nature 2020;587:54–8.
[19] Bochenek CD, Ravi V, Belov KV, et al. A fast radio burst associated with a Galactic magnetar. Nature 2020;587:59–62.
[20] Zhang B. The physics of fast radio bursts. Rev Mod Phys 2023;95:035005.
[21] Wadiasingh Z, Timokhin A. Repeating fast radio bursts from magnetars with low magnetospheric twist. Astrophys J 2019;879:4.
[22] Wang W, Luo R, Yue H, et al. FRB 121102: A starquake-induced repeater? Astrophys J 2018;852:140.
[23] Popov S B, Postnov K. Hyperflares of SGRs as an engine for millisecond extragalactic radio bursts. arXiv e-prints 07102006 2007.
[24] Dai ZG. A magnetar-asteroid impact model for FRB 200428 associated with an X-ray burst from SGR 1935+2154. Astrophys J Lett 2020;897:L40.
[25] Zhang B. A "Cosmic Comb" Model of Fast Radio Bursts. Astrophys J Lett 2017;836:L32.
[26] Hutton K, Woessner J, Hauksson E. Earthquake monitoring in Southern California for seventy-seven years (1932–2008). Bull Seismol Soc Am 2010;100:423–46.
[27] Båth M. Earthquake energy and magnitude. Phys Chem Earth 1966;7:115–65.
[28] Watanabe K, Masuda S, Segawa T. Hinode flare catalogue. Sol Phys 2012;279:317–22.
[29] Wang FY, Yu H. SGR-like behaviour of the repeating FRB 121102. J Cosmol Astropart Phys 2017;2017:023.
[30] Oppermann N, Yu HR, Pen UL. On the non-Poissonian repetition pattern of FRB121102. Mon Not R Astron Soc 2018;475:5109–15.
[31] Hewitt DM, Snelders MP, Hessels JWT, et al. Arecibo observations of a burst storm from FRB 20121102A in 2016. Mon Not R Astron Soc 2022;515:3577–96.
[32] Cruces M, Spitler LG, Scholz P, et al. Repeating behaviour of FRB 121102: Periodicity, waiting times, and energy distribution. Mon Not R Astron Soc 2021;500:448–63.
[33] Jahns JN, Spitler LG, Nimmo K, et al. The FRB 20121102A November rain in 2018 observed with the Arecibo Telescope. Mon Not R Astron Soc 2023;519:666–87.
[34] Wang FY, Wu Q, Dai ZG. Repeating fast radio bursts reveal memory from minutes to an hour. Astrophys J Lett 2023;949:L33.
[35] Totani T, Tsuzuki Y. Fast radio bursts trigger aftershocks resembling earthquakes, but not solar flares. Mon Not R Astron Soc 2023;526:2795–811.
[36] Omori F. On the after-shocks of earthquakes. Ph.D. thesis. Tokyo: The University of Tokyo; 1895.
[37] Kagan YY, Knopoff L. Spatial distribution of earthquakes: The two-point correlation function. Geophys J 1980;62:303–20.
[38] Lippiello E, de Arcangelis L, Godano C. Influence of time and space correlations on earthquake magnitude. Phys Rev Lett 2008;100:038501.
[39] Saichev A, Sornette D. Theory of earthquake recurrence times. J Geophys Res Solid Earth 2007;112:B04313.
[40] Pincus SM. Approximate entropy as a measure of system complexity. Proc Natl Acad Sci USA 1991;88:2297–301.
[41] Delgado-Bonal A. Quantifying the randomness of the stock markets. Sci Rep 2019;9:12761.
[42] Cencini M, Cecconi F, Vulpiani A. Chaos: From Simple Models to Complex Systems. Singapore: World Scientific; 2010.
[43] Schölzel C. Nonlinear measures for dynamical systems, 2019.
[44] Zhang YK, Wang P, Feng Y, et al. FAST observations of an extremely active episode of FRB 20201124A. II. energy distribution. Res Astron Astrophys 2022;22:124002.
[45] Zhang YK, Li D, Zhang B, et al. FAST observations of FRB 20220912A: Burst properties and polarization characteristics. Astrophys J 2023;955:142.

Yong-Kun Zhang is a Ph.D. candidate at National Astronomical Observatories, Chinese Academy of Sciences. He obtained his Bachelor's degree in Physics from University of Chinese Academy of Sciences in 2019. His current research interest includes fast radio bursts, star formation, and applications of machine learning in astronomy.

Di Li is the Chief Scientist of the radio division of the National Astronomical Observatories, Chinese Academy of Sciences. He has been the chief scientist of FAST since 2018. He received his Bachelor's degree in Physics from Peking University in 1995 and Ph.D. degree in Astrophysics from Cornell University in 2002. His research work includes star formation, fast radio bursts, pulsars, gravitational waves, astrochemistry, and radio astronomy techniques.